Research Article | Vol. 27, No. 11 | 27 May 2019 | OPTICS EXPRESS 15943
Optics EXPRESS

Quality and parameter control of X-ray absorption gratings by angular X-ray transmission

NIKOLAI GUSTSCHIN,[1,4,*] ALEX GUSTSCHIN,[1,4] PASCAL MEYER,[2] MANUEL VIERMETZ,[1] PHILIPP RIEDERER,[1,2] JULIA HERZEN,[1] JÜRGEN MOHR,[2] AND FRANZ PFEIFFER[1,3]

[1] *Chair of Biomedical Physics, Department of Physics and Munich School of BioEngineering, Technical University of Munich, 85748 Garching, Germany*
[2] *Institute of Microstructure Technology, Karlsruhe Institute of Technology, 76344 Eggenstein-Leopoldshafen, Germany*
[3] *Department of Diagnostic and Interventional Radiology, Klinikum rechts der Isar, Technical University of Munich, 81675 München, Germany*
[4] *These authors contributed equally to this work.*
[*] *nikolai.gustschin@tum.de*

Abstract: Here we report on a non-destructive, spatially resolving and easy to implement quality and parameter control method for high aspect ratio X-ray absorption gratings. Based on angular X-ray transmission measurements, our proposed technique allows to determine the duty cycle, the transmittance, the height, as well as the local inclination of the absorbing grating structures. A key advantage of the presented method is a fast and extensive grating quality evaluation without the need of implementing an entire grating interferometer. In addition to the local and surface-based analysis using a scanning electron microscope, our non-destructive method provides global averaged macroscopic and spatially resolved grating structure information without the requirement of resolving individual grating lines.

1. Introduction

Imaging and sensing techniques based on refraction and scattering of light found countless applications in science and technology. In the last two decades, much effort has been invested to extend these modalities to the X-ray regime and exploit the penetrative properties of X-rays for phase-sensitive imaging [1–5]. Among different technical methods, the grating-based approach gained strong interest because of its wide availability and its flexibility in system design. After the first studies at synchrotron facilities [1] the method was extended to work with incoherent, polychromatic X-ray sources, utilizing the principle of a Talbot-Lau interferometer [2]. Further, an additional dark field signal sensitive to small angle X-ray scattering was extracted from the interferometric data [3]. Many potential applications towards clinical imaging [4–6], nondestructive testing [7], security screening [8] and others have been reported.

A typical realization of such an imaging device requires one phase-shifting and two absorbing gratings consisting of periodical line arrays in the micrometer range. At first, an absorbing grating (G0) close to the X-ray source is used to create many equidistant line sources, which provide spatial coherence required for the interferometer. Then, a phase grating (G1) is used as a beam splitter to impose a relative periodical phase shift to the wave-front, which then results in an interference pattern according to the Talbot-Effect. Since the lateral intensity variations are too small to be resolved with standard X-ray detectors, the periodic interference pattern is analyzed by a second absorption grating (G2) in front of the detector. By linear stepping of one of the gratings in the range of one grating period and acquiring the respective radiograph at each

#355372 https://doi.org/10.1364/OE.27.015943
Journal © 2019 Received 13 Dec 2018; revised 15 Feb 2019; accepted 17 Feb 2019; published 21 May 2019

Optics EXPRESS

step, the fringe intensity modulation is recorded for every pixel. A comparison with a reference scan without the sample yields additional information about the phase-shifting and scattering characteristics of the examined object [2, 3].

The major technical challenge in the implementation of such imaging systems is the fabrication of the absorbing gratings. Especially for the hard X-ray regime (>60 kV tube acceleration voltage) relevant for clinical application, structures with a very high aspect ratio (AR) are required. Since the typical grating periods are in the range of 2–40 µm and absorbing heights up to several hundred µm are desired for a reasonable performance, only a few micro-fabrication techniques can approach that task. The key challenge lies in the precise fabrication of a binary grating profile with extremely perpendicular sidewalls which can then be filled by electroplating or other metalization techniques. The required grating structure can either be achieved by Deep X-ray Lithography (DXRL) [9, 10] or different anisotropic silicon etching techniques [11, 12]. In Deep Reactive Ion Etching (DRIE) a precisely controlled alternation of etching and sidewall passivation steps is required to achieve a high etching anisotropy. In particular, reaching a highly perpendicular sidewall angle is delicate since the profile tends to change with depth and is therefore aspect ratio dependent [12]. Alternatively, high AR gratings in silicon can be realized by anisotropic wet etching of 110 silicon substrates with KOH or TMAH making use of different etching rates along the crystallographic planes yielding excellent vertical sidewalls [11]. The filling of the absorber material can be performed by electroplating after deposition of plating contacts which seems to be the limiting factor in AR [11]. Other metalization techniques like Atomic Layer Deposition (ALD) [13], microcasting [14, 15] or hot embossing [16, 17] have been approached to increase AR and could possibly make the fabrication process simpler and more cost effective. Grating fabrication based on the LIGA (German acronym for Lithographie, Galvanoformung, Abformung) process, however, uses a conductive substrate with thick resist layers which are structured by DXRL. Since the lithographic step is performed with highly parallel X-ray radiation provided at synchrotron beamlines very high AR (up to 1:100) can be achieved [9]. For both the silicon-etched as well as LIGA-fabricated gratings the sidewall inclination is a crucial parameter since already at little deviation from the ideal perpendicular shape the transmittance of the grating strongly decreases. In one example given later in Fig. 3(a), a deviation of 0.3° from the ideal orientation results in a loss of more than 10 % of intensity which is extremely inconvenient for dose-critical clinical applications. Hence, a fast, non-destructive, large area and spatially resolving method for sidewall inclination as well as absorber height measurements of high AR gratings is of great benefit.

Currently, SEM (scanning electron microscopy) is routinely applied to visualize the surface of gratings, however, provides only 2D information from the surface or the profile at a cleaved edge. In particular, a complete analysis of the entire grating area in terms of high resolution SEM micrographs for quality control would be extremely time consuming and data-heavy. Cross-sectional SEM micrographs visualizing the grating profile are further destructive and show the profile only along one certain cleaved edge.

A sound characterization of absorption gratings can be performed by visibility tests in a grating interferometer. This requires, however, an entire reference setup of two or three gratings, which has typical lengths of 2 m for the hard X-ray regime and therefore cannot be performed in most commercial X-ray imaging systems. Further, the visibility results also depend on many parameters such as X-ray spectrum, interferometer geometry, alignment precision, local quality variations of the other gratings in use as well as the detector type. In particular, poor visibility results in most cases do not provide direct information about what particular grating parameter is responsible for the result.

A non-destructive method for the height determination of high AR absorbing gratings was recently reported [18]. By radiographic measurement of the Angular X-ray Transmission (AXT) of the grating, minima and maxima occur under certain angles which directly relate to the

Optics EXPRESS

period-to-height ratio. Since the period is usually known with a high precision the height can be calculated assuming a well-shaped grating profile.

In this work, we first extend the method to a cone beam geometry which makes it possible to use short imaging devices (<1 m) such as commercial microCT systems. In addition, we extract further useful parameters and quality criteria from the AXT curve. In particular, we reconstruct a shadowing-corrected, spatially resolved transmittance and absorber height of the grating. This tool is very useful to study and control the absorber deposition process as it can provide quantitative information on how homogeneous and high the absorbing material was deposited in the grating structure. Further, we visualize and quantify local variations in the inclination angle of the absorbing lamellae structures with a high precision. Our pixel-wise data evaluation routine yields spatially resolved information and does not require precise knowledge about the spectrum or detector characteristics of the imaging system. The presented analysis provides a time- and cost-effective routine for quality control as well as valuable information for fabrication process development.

2. Method

2.1. Angular X-ray transmission

The angular transmittance T_α of an X-ray beam through a binary absorbing grating structure is defined as the intensity I_α transmitting the grating in a certain angle α normalized to the incoming intensity I_0. The effective absorber height is the geometrical path length through absorber material under the angle α to the grating surface normal, as illustrated in Fig. 1 for three different incident angles. This effective height is a function of α, the period p, the duty cycle d (fraction of the absorbing line area) and the height h of the absorbing lines. It forms a periodical profile along the substrate axis x (see Fig. 1) and should be denoted as $H(\alpha, x, p, d, h)$. The energy-dependent transmittance by this effective height profile is calculated by integration over one period p and application of the Lambert-Beer law:

$$T_\alpha(E, \alpha, p, d, h) = \frac{I_\alpha(E, \alpha, p, d, h)}{I_0} = \int_0^p \exp(-\mu(E) H(\alpha, x, p, d, h))\, \mathrm{d}x, \tag{1}$$

for the energy E with the energy-dependent linear attenuation coefficient $\mu(E)$. Assuming the use of a polychromatic source with energy-normalized spectrum $S(E)$ and an energy integrating detector with quantum efficiency $D(E)$, the transmittance is:

$$T_{\alpha,\mathrm{poly}}(E, \alpha, p, d, h) = \int_0^{E_{\max}} T_\alpha(E, \alpha, p, d, h) E S(E) D(E)\, \mathrm{d}E. \tag{2}$$

Here, the attenuation by the grating substrate can be considered in good approximation as a filtration of the spectrum $S(E)$. Note that we neglect scattering effects due to their isotropic nature and significantly lower interaction cross section for the relevant energy range and materials (e.g. Si and Au). In the following, we will discuss different grating parameters and their influence on T_α to extract valuable information from AXT measurements.

2.2. Transmittance and cone beam distortion correction

One of the most important grating parameters is the transmittance, meaning the fraction of transmitted radiation impinging perpendicularly on the grating. It depends strongly on the duty cycle and the height of the absorbing structures as well as the thickness and material of the

Optics EXPRESS

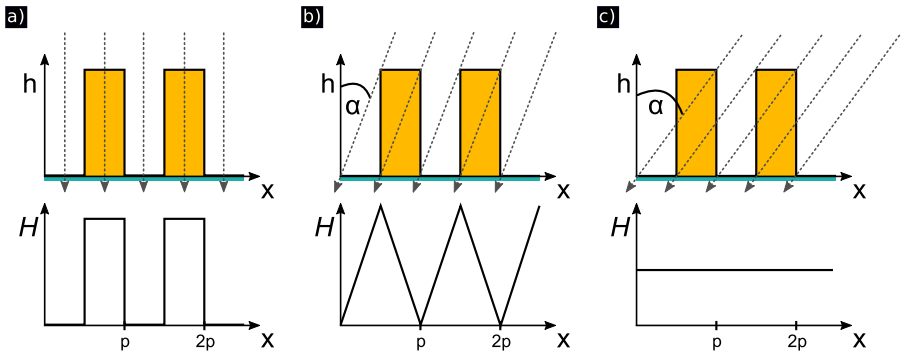

Fig. 1. The projected height profile H of a grating strongly depends on the angle of incidence of the radiation. The top part of (a)-(c) shows a sketch of a grating segment which is illuminated perpendicularly to the substrate in (a) and at an angle $\alpha \neq 0$ relative to the grating lamellae in (b) and (c). The bottom part shows the projected height profile H onto the substrate, respectively.

grating substrate. A 2D transmittance image of the grating can apparently reveal local variations of structure quality and is therefore of great interest. At a parallel beam setup, the transmittance image can be acquired in a single radiograph. In case of a cone beam, only the narrow, central part of the beam will impinge parallel to the grating lamellae. The outer parts of the beam will be shadowed by the absorbing structures as shown in Figs. 1(b) and 1(c). Therefore, the acquisition of a transmittance image is not straight forward. A convenient solution is to only use a small field of view where the cone beam can be neglected. In this approach one has to stitch many projections during a linear movement of the grating perpendicular to the beam axis. This method is quite time-consuming and returns only the 2D transmittance image.

We suggest a more elaborate approach, which uses AXT data from one single measurement to reconstruct not only the 2D transmittance, but also other highly relevant parameters of the analyzed grating. It requires preprocessing of the AXT data because when short setups are used and grating dimensions in the range of 10 cm and more are to be analyzed, the paraxial approximation cannot be applied anymore as in the previous work [18]. During the rotational movement of the grating, a specific grating coordinate is projected onto different detector pixels as illustrated in Fig. 2. A pixel-wise determination of a certain grating parameter (e.g. transmittance) from the AXT curve results in a geometrically distorted 2D image. To correct for the grating movement during the measurement we apply a projective transformation on every angular radiograph considering the setup geometry.

An extraction of the detector signal for every pixel P_{ij} at an angle $\alpha_{\parallel}$ where the grating substrate is oriented perpendicular to the cone beam impinging on the respective pixel yields a cone beam- and distortion-corrected transmittance image. Although this image already enables an assessment of the grating structure quality, a quantitative analysis is challenging due to mainly two difficulties. First, the grating transmittance is an energy-dependent property and consists of a part transmitting the transparent grating area and a second part transmitting the absorbing grating lines. Both contributions are also attenuated by the substrate and are weighted by the duty cycle of the grating. Second, the used X-ray spectrum is highly polychromatic and conventional flat-panel detectors only deliver energy-integrated count rates which are also biased by their energy-dependent quantum efficiency. Hence, the measured transmittance will always depend on the used spectrum and hardware of the imaging device.

Optics EXPRESS

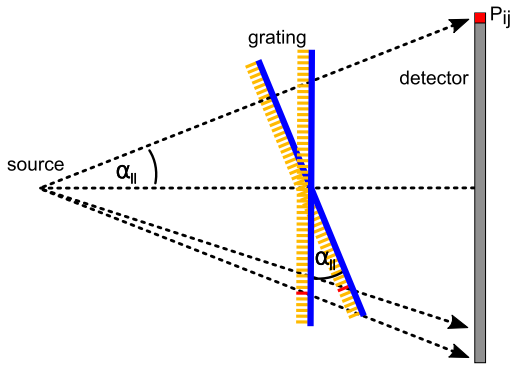

Fig. 2. Angular X-ray transmission (AXT) measurement geometry illustrating the movement of a probed grating area on the detector during a rotation of the grating (bottom). The maximal angular transmittance is reached at an angle $\alpha_{\parallel}$ where the grating lamellae are oriented parallel to the beam impinging on a certain pixel P_{ij} on the detector (top).

2.3. Duty cycle

As explained in the previous section, the grating duty cycle d (absorbing line width/period) has the main influence on the transmittance. Further, d is also a very sensitive parameter in interferometer performance [19] and therefore must be controlled with a high precision. The major influence of d on the AXT function is detectable at 0°. At angles in the range of higher order transmission maxima only little change is to be expected with variation of d [18]. One possible approach to reconstruct the duty cycle is to fit the measured AXT function based on Eq. (2), when the properties of the imaging system such as the X-ray spectrum are known and further factors such as grating substrate and the energy-dependent quantum efficiency of the detector are taken into account. However, for most commercially available X-ray imaging systems this information is hardly accessible without much effort which makes a quantitative retrieval of experimentally acquired AXT curves difficult. Further, the fitting process is unstable as well as computationally expensive and data-heavy, since the algorithm would have to perform a full polychromatic attenuation calculation at each iteration during pixel-wise cost function minimization or use large look-up tables for each parameter combination.

The problem is significantly reduced if a soft X-ray spectrum is used at which the absorbing grating lines almost completely attenuate the beam. For example using a 40 kVp tungsten spectrum, already 150 µm high Au bars absorb more than 99 % of the radiation allowing to neglect the residual transmission through the absorbing lines. To eliminate the absorbing influence of the substrate which becomes stronger at lower energies, the AXT radiographs are normalized to an area with unstructured substrate after the measurement. Alternatively, it is also possible to perform a flat-field correction with an equivalent unstructured substrate.

Combining both approaches, a low energy spectrum as well as a substrate-normalization, expected transmittance values close to $(1 - d)$ are achieved and provide a good estimate for the duty cycle.

2.4. Height of absorbing structures

As reported in a previous work [18], the period-to-height ratio of the grating structures can be extracted from the minima of the AXT curve which appear at rotation angles where $H = const.$ (see Fig. 1(c)):

$$\alpha_n = \tan^{-1}\left(n\frac{p}{h}\right), \tag{3}$$

Optics EXPRESS

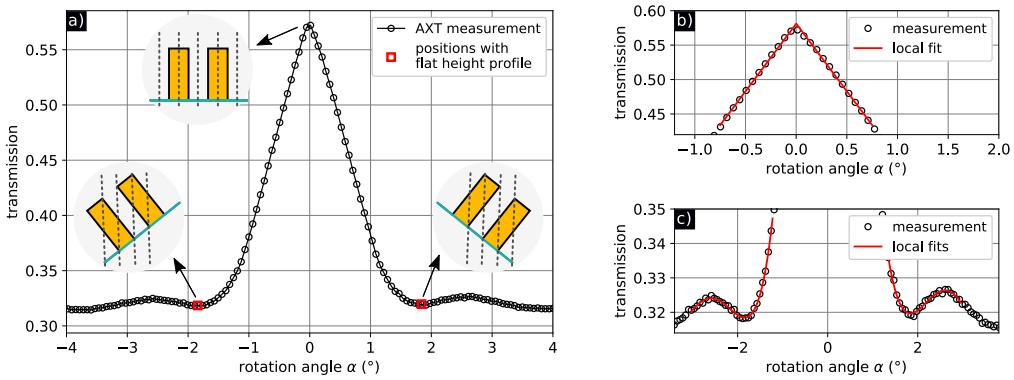

Fig. 3. (a) Measured Angular X-ray Transmission (AXT) profile of an absorption grating with 4.8 µm period and ~ 150 µm gold height. (b) Determination of maximum transmittance angle by locally fitting a triangular function to the tip of the curve. (c) First order transmission minima determination by local 3rd order polynomial fits.

where n is the order of the minimum. As this is due to a geometric effect, the angular positions of the minima are not affected by the used X-ray spectrum, duty cycle, grating substrate or detector type, but only depend on the period-to-height ratio. To obtain a spatially resolved height of the grating the minima of the cone-beam-corrected AXT curve have to be found for every pixel. As in the previous case, this can be performed by iteratively fitting the AXT function according to Eq. (2) if the properties of the imaging system are known. We found, however, that it is considerably more efficient to approach the task by local 3rd- or 4th-order polynomial fitting (shown in Fig. 3(c)) which provides the angular position of the first minimum for each pixel at low computational effort and good precision. From that value a full spatial representation of the grating height is reconstructed according to Eq. (3).

2.5. Local absorber inclination

We found that AXT measurements are well suited to determine small angle deviations of the lamellae from the ideal perpendicular orientation to the substrate. The principle is based on the observation that the maximal transmission signal in a pixel P_{ij} is recorded at an angle $\alpha_{\parallel}$ where the cone beam impinging on that pixel is parallel to the grating lamellae (see Fig. 2). Hence, the tip of the AXT curve is fitted by a triangular function as shown in Fig. 3(b) and the angle $\alpha_{\parallel}$ of the peak value is extracted in every pixel. Subsequently, the impinging angle α_c of the cone beam on each detector pixel is calculated from the geometrical arrangement of detector and X-ray source. The difference $\Delta\alpha = (\alpha_c - \alpha_{\parallel})$ is corresponding to the local inclination of the absorber lines from the ideal perpendicular orientation. As will be shown in the experimental section, this value can visualize small defects like cracks or waviness in the structure which are hardly seen in the reconstructed transmittance of the grating and difficult to quantify by microscopy-based surface analysis only. It also enables a quantitative, nondestructive and large area study of the lamellae inclination in grating fabrication processes where strong external forces [16, 17] or thermal fluctuations [14, 15] leading to mechanical deformations in the micrometer range have to be controlled.

Optics EXPRESS

Table 1. Grating and scanning parameters for the given examples. Gold heights are approximate values determined by SEM (scanning electron microscopy) during fabrication. The scan parameters are tube voltage, tube current and detector exposure time per image.

grating No.	period (µm)	duty cycle	height (µm)	substrate	scan settings (kV / µA / s)	angular range/step (°)
#1	10	0.51	190	silicon	40 / 200 / 2	-10 to 10 / 0.1
#2	10	0.69	220	graphite	40 / 200 / 2	-6 to 6 / 0.1
#3	45	0.50	300	graphite	100 / 220 / 5	-16 to 16 / 0.2
#4	4.8	0.50	145	graphite	80 / 160 / 5	-5.5 to 5.5 / 0.06

3. Experimental

3.1. AXT measurement

The grating characterization via AXT measurements is demonstrated with various grating samples in this study. The AXT measurements were performed on a phoenix|x-ray v|tome|x (General Electrics) system with a direct tungsten anode tube. The system is equipped with a flat-panel detector (1000 × 1000 pixels, 200 µm pixel size) allowing to analyze grating dimensions well above 10 cm × 10 cm. Depending on the requirements of data quality and resolution the typical total scan times are in the range of 10–60 minutes. The acquisition parameters for the different samples are given in Table 1. First, two gratings with 10 µm period, different duty cycles and substrates were scanned at low energy to show that quantitative determination of the DC is possible by a suitable AXT measurement. For both samples, the measurements were normalized to areas with unstructured substrate covered with resist. Since both gratings had stabilizing resist bridges between the transparent lines (which is common for LIGA-fabricated high AR gratings) the transmittance in the central beam is expected to be increased by approximately the bridge fraction (fraction of transparent bridge area of total grating area). To avoid this effect, the grating was placed in the center bottom of the detector field of view so that the impinging beam was inclined to the bridge orientation by about 4° in the analyzed area. Since the scanned gratings had a high AR this arrangement allowed to almost completely eliminate the influence of the additional transmittance by the bridges for an accurate duty cycle determination. Furthermore, an absorption grating piece with 4.8 µm period and crack defects was scanned to demonstrate the AXT-based height determination and defect visualization. A further absorption grating with 45 µm period and a strong height modulation along the entire grating area was scanned to demonstrate large area characterization. To verify the angular lamellae inclination data, some high resolution projections from slightly different angles of the same grating area were taken with a ZEISS Xradia 500 Versa microCT. The system is based on a microfocus X-ray tube and a scintillator-coupled CCD and is able to resolve individual grating lines. For the high resolution measurements, the field of view was centered around the rotation axis.

3.2. Analysis via microscopy

To verify the duty cycle and height determination obtained from AXT measurements, some independent methods were used. For the verification of the duty cycle five SEM images of grating #1 and #2 at random positions in the measured grating area were acquired, respectively. The duty cycle of the grating was measured at five random locations in every image.

For the height verification, a relative 2D height distribution at one distinct location of grating #3 was measured with a confocal microscopy-based profilometer (Microsurf, NanoFocus AG).

Optics EXPRESS

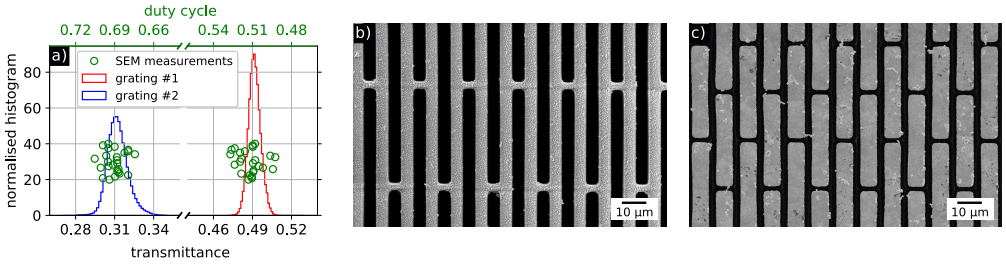

Fig. 4. Transmission-based duty cycle estimation of two gratings with different duty cycles and substrates. (a) Histograms of AXT-based transmission signal over an 2 cm × 2 cm grating area for gratings #1 and #2. In both histograms, the green circles depict SEM-based measurements of the duty cycle at multiple locations in the respective grating. The y-values for the green circles are insignificant but merely randomly selected for a better illustration of their distribution. (b) SEM micrograph of grating #1 (mapping the resist between the gold lamellae in white) and (c) grating #2 (mapping the gold lamellae).

The ROI with a strong height modulation on the grating was chosen to demonstrate the spatial precision of our AXT-based method. Secondly, the edge of grating #4 was analyzed by SEM to visualize the grating height and some surface defects. All SEM images were acquired with a JEOL JSM-6060LV (JEOL, Freising) scanning electron microscope.

4. Results and discussion

4.1. Duty cycle determination from transmittance

From the transmittance images obtained for gratings #1 and #2 histograms over an area of 2 cm × 2 cm are shown in Fig. 4(a). The mean transmittance values of both gratings are 0.49 for grating #1 and 0.31 for grating #2. The results match well with the duty cycles obtained from SEM micrographs (see Figs. 4(b) and 4(c)). Hence, an accurate determination of the spatially resolved duty cycle of gratings with different substrates is possible based on transmittance values determined with suitable scanning conditions. Note, however, that an abnormal variation of grating transmittance does not necessarily imply a variation of the duty cycle. It can be also caused by e.g. local overplating with the absorption material, strongly inclined sidewalls of the absorber or simply voids in the grating filling, which increase the transmittance signal. A homogeneous grating transmittance over the entire grating is on the other hand a clear indication of a constant duty cycle with perpendicular, well shaped absorbing grating lines. Therefore, the 2D transmittance image should be considered as the main quality control criteria of absorption gratings.

4.2. Height determination and verification

The first example of height determination by AXT is demonstrated with grating #4 with 4.8 µm period and a height of about 145 µm. In Fig. 5 the reconstructed transmittance 5(a), lamellae inclination 5(b) and grating height 5(c) are shown. The grating height was obtained by pixel-wise fitting the first order minimum of the corresponding AXT curve. The grating height of (145.0 ± 1.1) µm determined by AXT in the blue rectangle in Fig. 5(c) is in good agreement with the height of 147 µm determined from SEM images (Figs. 5(e) and 5(f)) which show the grating edge of the ROI depicted in Fig. 5(c).

As a second example the AXT analysis of grating #3 is shown in Fig. 6. Again, grating transmittance, absorber inclination and height were reconstructed. This example illustrates the

Optics EXPRESS

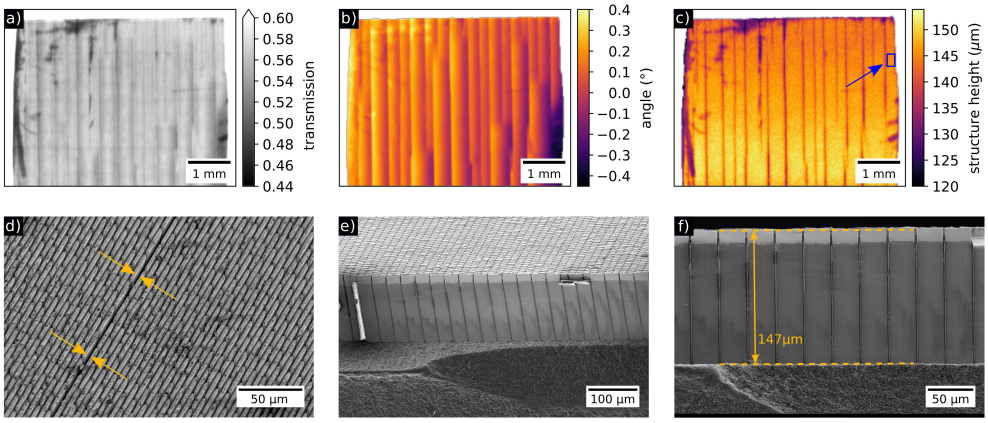

Fig. 5. Analysis of a 4.8 µm period grating piece (grating #4). (a) Transmission image, (b) inclination angle of the grating lamellae visualizing cracks in the grating structure and (c) spatially reconstructed lamellae height. (d) SEM image of a typical crack on the grating surface, (e) grating edge located at the marked rectangular area in (c) and (f) detailed view perpendicular on the grating lines depicting the height of the lamellae confirming the height obtained by AXT with a high precision.

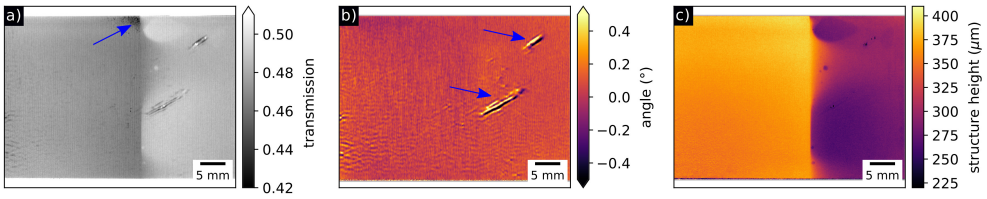

Fig. 6. Large area characterization of an absorption grating with 45 µm period (grating #3). (a) Transmittance, (b) Lamellae angle inclination map and (c) reconstructed structure height of the absorbing lamellae.

benefit of complementary parameter determination by AXT measurements. Variations seen in the transmittance (Fig. 6(a)) could be interpreted as duty cycle variations or poor grating quality due to local overplating or inclined lamellae. However, an additional look on the inclination map reveals that only the two defects outlined in Fig. 6(b) originate from not perfectly perpendicular lamellae. The other inhomogeneities in the transmittance are related to height variations as can be seen in the height map in Fig. 6(c). Note, that the defect outlined by the arrow in the upper center of the transmittance map does neither show up in the inclination nor in the height map. It is attributed to local Au overplating as could be confirmed by light microscopy. To estimate the spatial resolution of the AXT-based height determination the abrupt height decrease in the center of the grating is analyzed further. Figure 7(a) shows the AXT height data correlated with the grating profile measured by the profilometer. Figure 7(b) displays the topography of the grating surface resolving the height of individual grating lines. Note, that the data obtained from confocal height measurement was leveled to the absolute height obtained from the AXT data, as the profilometer is not able to detect the entire profile down to the bottom of the grating due to its

Optics EXPRESS

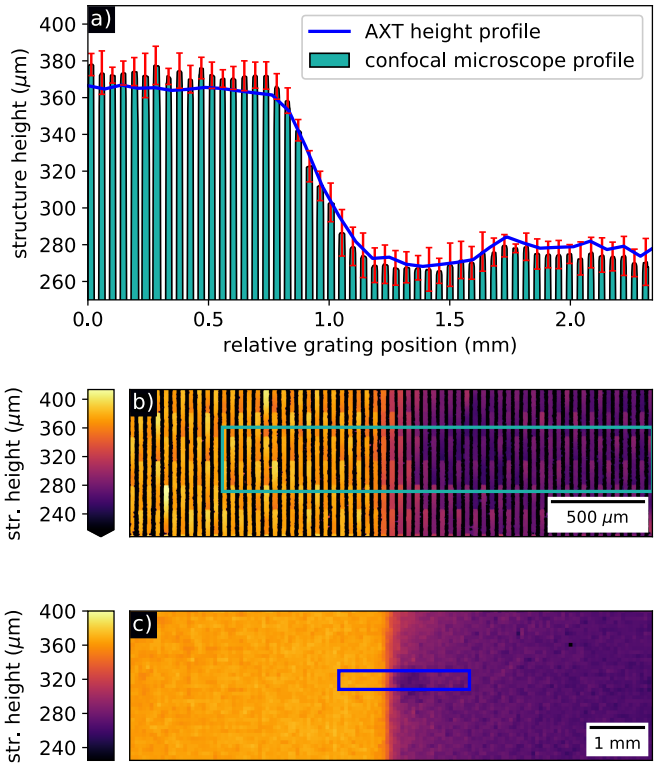

Fig. 7. (a) Comparison of AXT-based grating height determination with high resolution data obtained by confocal microscopy. The error bars give the standard deviation of the grating height along the averaged ROI. (b) Grating surface topography resolving individual grating lines. The depicted rectangle shows the ROI along the profile in (a) was averaged. (c) AXT-based height map reconstruction showing the same ROI which was analyzed by the newly described method. The data shows that AXT measurements can detect height variations with sub-mm lateral resolution on large grating areas.

high AR. Figure 7(c) shows the height distribution obtained by AXT of the same area. Both 7(b) and 7(c) are equally color-coded in height to illustrate the conformity with both measurement methods. The error bars given in 7(a) denote the standard deviations of grating height obtained from averaging along the depicted ROI in 7(b).

This example shows that our method can quantitatively visualize local grating height variations with a resolution well below 1 mm on large grating areas.

4.3. *Absorber inclination and verification*

Grating #4 is an example where linear variations of the absorber inclination angle in the range of $-0.4°$ to $0.4°$ are revealed by the AXT analysis (Fig. 5(b)). This alternations are caused by cracks in the resist structure as seen in the SEM micrograph in Fig. 5(d) and are attributed to resist shrinkage. They introduce local modulations of the grating period and duty cycle and should therefore be avoided to prevent artefacts in the images. As expected, this local discontinuities in periodicity are causing artefacts in the height map (Fig. 5(c)) since it is directly calculated from a known period by Eq. (3). Further artefacts are seen in both the transmittance and height at the

Optics EXPRESS

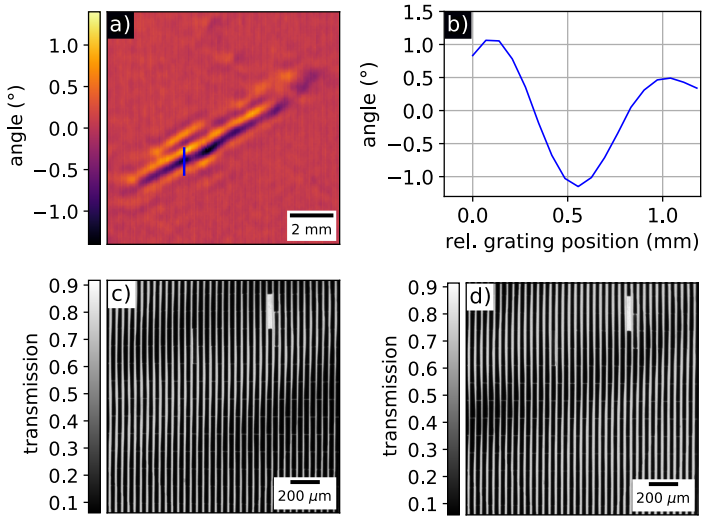

Fig. 8. (a) AXT-based lamellae inclination angle determination showing a defect (waviness) in the grating structure. (b) shows a plot of inclination angle along the blue line in (a). The AXT-based findings are confirmed by (c) and (d) showing high resolution X-ray projections of the same grating area from slightly different angles (−1.1° (c) and 1.1° (d)).

left grating border and top left in Figs. 5(a) and 5(c). Since these artefacts are not pronounced in the inclination map, their origin does not lie deep in the grating structure but is rather caused by defects on the grating surface like scratches or overplating with absorbing material.

In a second example a defect in grating #3 which is visible in Fig. 6(b) is analyzed. Figure 8(a) shows the absorber inclination angle of one of the two defects in detail. A line plot of the angle along the blue line is shown in Fig. 8(b) and shows modulations of up to more than 2°. To verify the angle data obtained by AXT we acquired high resolution X-ray transmission images in the region of the line plot resolving individual grating lines. Figures 8(c) and 8(d) show two microradiographs of the same grating area rotated by 2.2° with respect to each other (difference range of the angle observed in 8(b)). They reveal that areas which are shadowed by inclined grating lines in one image show maximal transmittance in the other. Thus, AXT is capable of providing reliable data on the inclination angle of the grating lamellae.

4.4. Limitations

As the presented AXT method acquires averaged data from periodic absorbing microstructures, it has several limitations originating from the applied principles. At first, the grating has to have a sufficiently high AR (ideally > 10) and strongly absorbing material to deliver enough contrast for the formation of angular transmittance minima according to Eq. (2). Further, the grating must have approximately uniform structure at least on the range of the pixel size of the measurement system. Apparently, e.g. differently inclined absorber lines on an area imaged by a single pixel will not be resolved but averaged. However, this will result in a decreased transmission signal and will be still detectable as an abnormality. This might be relevant for gratings etched by DRIE as the resulting trenches are often not perfectly perpendicular but have a slightly trapezoidal profile. As the trenches in this case are not inclined in a single direction the slope angle of the sidewall will not be revealed by AXT. However, the height determination can be also performed with slightly trapezoidal profiles as the position of the AXT minimum is hardly dependent on small slope angle variations.

Optics EXPRESS

5. Conclusion

We have presented a non-destructive and spatially resolving quality and parameter control method for X-ray absorption gratings which can be applied with widely used X-ray imaging equipment in short geometries. It provides a transmittance image which is sensitive to small deficiencies in the grating structure. Under suitable scanning conditions, the transmittance can deliver quantitative and spatially resolved data on the duty cycle of the grating, without the need to resolve individual grating lines. The height of the absorbing lamellae is reconstructed from angular transmission minima and can be analyzed over a large area non-destructively. Further, the inclination of the absorbing lamellae to the substrate on the entire grating is provided with high precision. The combination of the acquired parameters allows to perform a reliable quality assurance procedure without the need of an entire grating interferometer setup.

We expect the method to be very beneficial for future grating development as it addresses technical key challenges faced in state-of-the-art grating fabrication. To realize clinically applicable grating-based X-ray imaging systems a large field of view of a few tens of cm is a major concern. Hence, recent studies focus on the increase of the grating area [20–22] e.g. by stitching and gluing of several grating tiles on a large carrier substrate. Further, for some imaging setups, the planar grating substrate has to be bent to adapt the cone beam geometry of conventional X-ray sources. In this cases AXT analysis will provide quantitative feedback to study the bending behavior and to reduce potential discontinuities in absorber inclination angle at the edges of individual stitched grating tiles. We see further potential of the method to study alternative metallization techniques which use thermal and mechanical processes [14, 16, 17] to deposit the absorbing material into high AR grating structures. Typical defects such as partially filled trenches, quenched lamella or cracks in the grating structure can be visualized and characterized easier.

Generally, the method can be used to obtain quantitative structural information of different kinds of periodic absorbing structures (e.g. anti-scatter grids for radiography).

Funding

European Research Council (ERC) (AdG 695045).

Acknowledgments

This work was carried out with the support of the Karlsruhe Nano Micro Facility (KNMF, www.kit.edu/knmf), a Helmholtz Research Infrastructure at Karlsruhe Institute of Technology (KIT, www.kit.edu).

References

1. A. Momose, S. Kawamoto, I. Koyama, Y. Hamaishi, K. Takai, and Y. Suzuki, "Demonstration of x-ray talbot interferometry," Jpn. J. Appl. Phys. **42**, L866–L868 (2003).
2. F. Pfeiffer, T. Weitkamp, O. Bunk, and C. David, "Phase retrieval and differential phase-contrast imaging with low-brilliance x-ray sources," Nat. Phys. **2**, 258–261 (2006).
3. F. Pfeiffer, M. Bech, O. Bunk, P. Kraft, E. F. Eikenberry, C. Brönnimann, C. Grünzweig, and C. David, "Hard-X-ray dark-field imaging using a grating interferometer," Nat. Mater. **7**, 134–137 (2008).
4. A. Bravin, P. Coan, and P. Suortti, "X-ray phase-contrast imaging: from pre-clinical applications towards clinics," Phys. Med. Biol. **58**, R1–R35 (2013).
5. F. Pfeiffer, J. Herzen, M. Willner, M. Chabior, S. Auweter, M. Reiser, and F. Bamberg, "Grating-based x-ray phase contrast for biomedical imaging applications," Z. Med. Phys. **23**, 176–185 (2013).
6. F. Pfeiffer, "Milestones and basic principles of grating-based x-ray and neutron phase-contrast imaging," AIP Conf. Proc. **1466**, 2–11 (2012).
7. V. Ludwig, M. Seifert, T. Niepold, G. Pelzer, J. Rieger, J. Ziegler, T. Michel, and G. Anton, "Non-Destructive Testing of Archaeological Findings by Grating-Based X-Ray Phase-Contrast and Dark-Field Imaging," J. Imaging **4**, 58 (2018).
8. E. A. Miller, T. A. White, B. S. McDonald, and A. Seifert, "Phase contrast x-ray imaging signatures for security applications," IEEE Trans. Nucl. Sci. **60**, 416–422 (2013).

Optics EXPRESS

9. J. Mohr, T. Grund, D. Kunka, J. Kenntner, J. Leuthold, J. Meiser, J. Schulz, and M. Walter, "High aspect ratio gratings for X-ray phase contrast imaging," AIP Conf. Proc. **1466**, 41–50 (2012).
10. P. Meyer and J. Schulz, "Deep x-ray lithography," in *Micro-Manufacturing Engineering and Technology,*, 2nd ed., Y. Qin, ed. (Elsevier, 2015), Chap. 16, pp. 365–392.
11. C. David, J. Bruder, T. Rohbeck, C. Grünzweig, C. Kottler, A. Diaz, O. Bunk, and F. Pfeiffer, "Fabrication of diffraction gratings for hard X-ray phase contrast imaging," Microelectron. Eng. **84**, 1172–1177 (2007).
12. B. Wu, A. Kumar, and S. Pamarthy, "High aspect ratio silicon etch: A review," J. Appl. Phys. **108**, 051101 (2010).
13. J. Vila-Comamala, L. Romano, V. Guzenko, M. Kagias, M. Stampanoni, and K. Jefimovs, "Towards sub-micrometer high aspect ratio x-ray gratings by atomic layer deposition of iridium," Microelectron. Eng. **192**, 19–24 (2018).
14. Y. Lei, Y. Du, J. Li, Z. Zhao, X. Liu, J. Guo, and H. Niu, "Fabrication of x-ray absorption gratings via micro-casting for grating-based phase contrast imaging," J. Micromech. Microeng. **24**, 015007 (2014).
15. Y. Lei, X. Liu, J. Li, J. Guo, and H. Niu, "Improvement of filling bismuth for x-ray absorption gratings through the enhancement of wettability," J. Micromech. Microeng. **26**, 065011 (2016).
16. L. Romano, J. Vila-Comamala, H. Schift, M. Stampanoni, and K. Jefimovs, "Hot embossing of Au- and Pb-based alloys for x-ray grating fabrication," J. Vac. Sci. Technol. B **35**, 06G302 (2017).
17. L. Romano, J. Vila-Comamala, M. Kagias, K. Vogelsang, H. Schift, M. Stampanoni, and K. Jefimovs, "High aspect ratio metal microcasting by hot embossing for X-ray optics fabrication," Microelectron. Eng. **176**, 6–10 (2017).
18. M. Schüttler, P. Meyer, F. Schaff, A. Yaroshenko, D. Kunka, H. Besser, F. Pfeiffer, and J. Mohr, "Height control for small periodic structures using x-ray radiography," Meas. Sci. Technol. **27**, 025015 (2016).
19. M. Chabior, M. Schuster, M. Goldammer, C. Schroer, and F. Pfeiffer, "Influence of the grating profiles on the image quality in grating-based x-ray imaging," Nucl. Instrum. Meth. A **683**, 71–77 (2012).
20. T. J. Schröter, F. Koch, P. Meyer, M. Baumann, D. Münch, D. Kunka, S. Engelhardt, M. Zuber, T. Baumbach, and J. Mohr, "Large area gratings by x-ray liga dynamic exposure for x-ray phase-contrast imaging," J. Micro-Nanolith. Mem. **16**, 013501 (2017).
21. T. J. Schröter, F. J. Koch, D. Kunka, P. Meyer, S. Tietze, S. Engelhardt, M. Zuber, T. Baumbach, K. Willer, L. Birnbacher, F. Prade, F. Pfeiffer, K. M. Reichert, A. Hofmann, and J. Mohr, "Large-area full field x-ray differential phase-contrast imaging using 2D tiled gratings," J. Phys. D: Appl. Phys. **50**, 225401 (2017).
22. T. J. Schröter, F. J. Koch, P. Meyer, D. Kunka, J. Meiser, K. Willer, L. Gromann, F. de Marco, J. Herzen, P. Noel, A. Yaroshenko, A. Hofmann, F. Pfeiffer, and J. Mohr, "Large field-of-view tiled grating structures for X-ray phase-contrast imaging," Rev. Sci. Instrum. **88**, 015104 (2017).